Cross-link relations between π and ρ-meson channels and the QCD vacuum

S. V. Mikhailov[1,*] and N. G. Stefanis[2,†]

[1]*Bogoliubov Laboratory of Theoretical Physics, JINR, 141980 Dubna, Russia*
[2]*Ruhr-Universität Bochum, Fakultät für Physik und Astronomie, Institut für Theoretische Physik II, D-44780 Bochum, Germany*

(Received 12 July 2021; accepted 18 October 2021; published 18 November 2021)

We discuss cross-link relations between the π and ρ-meson channels emerging from two different descriptions of the QCD vacuum: instanton physics and QCD sum rules with nonlocal condensates (NLCs). We derive in both schemes an intriguing linear relation between the π and the $\rho^{\parallel}$-meson distribution amplitudes in terms of their conformal coefficients and work out the specific impact of the scalar NLC in these two channels. Using a simple model with Gaussian decay of the scalar NLC, we are able to relate it to the moments of the pion nonsinglet parton distribution function measurable in experiment—a highly nontrivial result. The implications for the pion and the $\rho^{\parallel}$-meson distribution amplitudes entailed by the obtained cross-link relations are outlined in terms of two generic scenarios.

DOI: 10.1103/PhysRevD.104.096013

I. INTRODUCTION

Recently, Polyakov and Son [1] have employed the instanton approach in combination with dispersion relations for the two-pion distribution amplitude (DA) [2] to obtain model-independent relations for the ratio $a_2^{(\rho)}/a_2^{(\pi)}$. Within this approach, the Gegenbauer moments of the ρ-meson DA can be expressed in terms of the two-pion distribution amplitudes (2πDAs). Using the conformal expansion

$$\varphi_{\pi(\rho)}^{(\mathrm{tw}-2)}(x,\mu^2) = \psi_0(x) + \sum_{n=2,4,\ldots}^{\infty} a_n(\mu^2)\psi_n(x) \qquad (1)$$

with the Gegenbauer basis

$$\psi_n(x) = 6x\bar{x}C_n^{(3/2)}(x-\bar{x}), \qquad (2)$$

where $\varphi_\pi^{\mathrm{asy}} = \psi_0(x) = 6x(1-x) \equiv 6x\bar{x}$ is the asymptotic pion DA, it was found that $a_2^{(\rho)}$ and $a_2^{(\pi)}$ are linearly related. It was argued that this is deeply rooted in chiral dynamics and the general properties of quantum field theory (QFT), such as unitarity, crossing, and dispersion relations. Going one step further, they used the soft pion theorem and the crossing symmetry [2] to relate the second Gegenbauer coefficient $a_2^{(\rho)}$ of the ρ-meson DA to the third Mellin moment of the pion valence-quark parton distribution function (PDF) measured in deep inelastic scattering (DIS). Referring for the full derivation to Ref. [1], one obtains the following relation:

$$\begin{aligned} a_2^{(\rho)} &= B_{21}(0)\exp\left(c_1^{(21)}m_\rho^2\right) \\ &= \left(a_2^{(\pi)} - \frac{7}{6}M_3^{(\pi)}\right)\exp\left(c_1^{(21)}m_\rho^2\right). \end{aligned} \qquad (3)$$

The main ingredient in the last equation is the measurable quantity

$$M_3^{(\pi)} = \int_0^1 dx x^2[q_\pi(x) - \bar{q}_\pi(x)], \qquad (4)$$

while $c_1^{(21)}$ is a low-energy subtraction constant in the dispersion relation for the generalized Gegenbauer moments $B_{nl}(W^2)$ used for the 2πDAs in Ref. [2] (see that reference for details). Fixing this constant by virtue of the instanton model of the QCD vacuum, one can determine the ratio $a_2^{(\rho)}/a_2^{(\pi)}$. To this end, we combine the value

$$a_2^{(\pi)}(\mu = 2\ \mathrm{GeV}) = 0.078 \pm 0.028, \qquad (5)$$

determined on the lattice with a next-to-leading-order (NLO) matching to the $\overline{\mathrm{MS}}$ scheme (adding the errors in quadrature) [3], with the value in the first line below,

$$M_3^{(\pi)}(\mu = 2\ \mathrm{GeV}) = \begin{cases} 0.114 \pm 0.020 & [4] \\ 0.110(7)(12) & [5], \end{cases} \qquad (6)$$

*mikhs@theor.jinr.ru
†stefanis@tp2.ruhr-uni-bochum.de

obtained at NLO in the phenomenological analysis in Ref. [4] within the xFitter framework. The second line shows the result of a recent lattice calculation [5]. One observes that the lattice estimate is within the error margin of the first line. This way, one gets [1]

$$\frac{a_2^{(\rho)}}{a_2^{(\pi)}}(\mu = 2\ \text{GeV}) = -(1.15 \pm 0.86)(1.0 \pm 0.1). \quad (7)$$

The above results provide the motivation for the present investigation with the attempt to derive similar linear relations between the π and ρ-meson channels within the QCD sum-rules approach with nonlocal condensates (NLC-SR for short) used in Ref. [6]. The key ingredients in NLC-SR are the nonlocal condensates [7–11]. In particular, the scalar NLC $\Phi_S(x, M^2)$, where M^2 is the Borel parameter, and the scale

$$\lambda_q^2 = \frac{\langle \bar{q} D^2 q \rangle}{\langle \bar{q} q \rangle}\bigg|_{\mu_0^2 \sim 1\ \text{GeV}^2} = 0.40 \pm 0.05\ \text{GeV}^2, \quad (8)$$

which defines the virtuality of vacuum quarks, are crucial for the determination of the shape of the pion DA employing NLC-SR [6,12].

This approach was originally used to derive a set of pion DAs [termed Bakulev-Mikhailov-Stefanis (BMS)] for $\lambda_q^2 = 0.40\ \text{GeV}^2$ in agreement with the CLEO experimental data [13] on the pion-photon transition form factor (TFF). It also provides good agreement with more recent data from Belle [14] and *BABAR* ($Q^2 \leq 9\ \text{GeV}^2$) [15]; see Ref. [16]. The coefficients $a_2^{(\pi)}$ and $a_4^{(\pi)}$ encapsulate the main theoretical characteristics of the nonperturbative QCD vacuum. Later, this scheme was employed in Ref. [17] to construct another variant of the pion DA with a platykurtic profile. This DA intrinsically combines two key features: end point suppression of the pion DA due to the vacuum quark virtuality $\lambda_q^2 = 0.45\ \text{GeV}^2$ and unimodality of the DA at $x = 1/2$, as found in the context of Dyson-Schwinger equations to account for the dynamically generated mass of the confined quark propagator; see Ref. [18] for a review. At the scale $\mu^2 = 4\ \text{GeV}^2$, one has the coefficients $(a_2^{(\pi)}, a_4^{(\pi)})_{\text{pk}}^{\mu^2} = (0.057, -0.013)$. This scheme [19] also provided a platykurtic DA for the longitudinally polarized ρ meson, $(a_2^{(\rho)}, a_4^{(\rho)})_{\text{pk}}^{\mu^2} = (0.017, -0.021)$, while previous attempts to construct the ρ-meson DA within this NLC-SR scheme were reported in Refs. [20,21].

The paper is structured as follows. In Sec. II, we compare the predictions for the $\pi - \rho$-meson coefficients following from Eq. (3) in Ref. [1]. We then derive an analogous expression to (3) using the NLC-SR scheme and discuss the dynamical difference of the impact of the scalar NLC in the axial and the vector channel. We also work out a linear relation between functionals depending on $\varphi_\rho^{\parallel}$ and φ_π and extend the result to higher orders of the conformal expansion. In Sec. III, we establish the linear relation between the π and ρ-meson DAs in terms of the specific characteristics of the NLC-SR. The ultimate goal of this section is to relate the scalar NLC to the third/fifth Mellin moment of the pion PDF. The implications of the negative sign of $a_2^{(\rho)}$ for the pion and $\rho^{\parallel}$-meson DAs are addressed in Sec. IV. Our conclusions are presented in Sec. V. The expressions for the scalar NLC are provided in Appendix A, while the correspondence between the instanton approach and the NLC-SR scheme is shown in Appendix B.

II. HOW TO RELATE THE $\rho^{\parallel}$ AND π DISTRIBUTION AMPLITUDES IN NLC-SR

It is instructive to compare the predictions for pairs $(a_2^{(\pi)}, a_2^{(\rho)})^{\mu^2}$, obtained within various approaches, with the cross-link relations following from Eq. (3). This is done in Fig. 1 in terms of the blue diagonal line, which represents the linear relation between such pairs.

The following results are displayed:

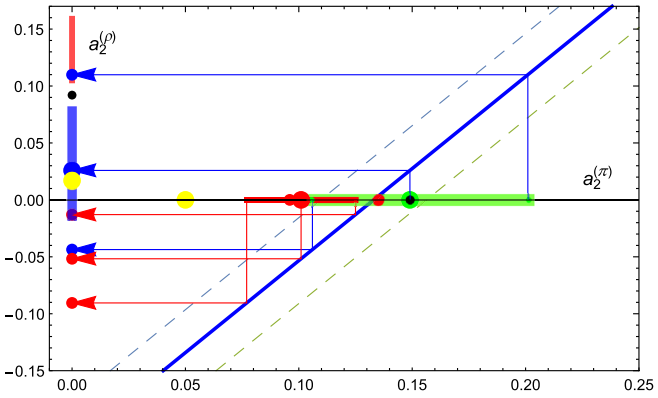

FIG. 1. Comparison of domains of pairs $(a_2^{(\pi)}, a_2^{(\rho)})$ obtained in different approaches at $\mu^2 = 4\ \text{GeV}^2$ obeying the linear relation given by Eq. (3). The blue diagonal line and the dashed lines around it originate from this relation and from the uncertainties of $M_3^{(\pi)}$ in (4). Lattice constraints for $a_2^{(\pi)}$ at NNLO provide the range [0.077, 0.125]—shown as a red segment with a central big red point along the horizontal axis. The N^{3}LO regime corresponds to the interval [0.096, 0.135] [3] limited by the red end points. The range $a_2^{(\rho)} = 0.132 \pm 0.027$ from Ref. [22] is shown as a short red segment at the upper end of the vertical axis. The NLC-SR fiducial regions are shown for the pion by the green segment [6] and for the $\rho^{\parallel}$-meson by the blue segment along the vertical axis [20]. The projections of the end points of the green segment and its center (green dot) are denoted by blue points on the $a_2^{(\rho)}$ axis. The yellow points mark the locations of the platykurtic pion and ρ DAs [17,19], respectively. The black points $a_2^{(\pi)} = 0.149$ and $a_2^{(\rho)} = 0.092$ denote the coefficients of the DSE DAs for π [23] and $\rho^{\parallel}$ [24].

(i) $a_2^{(\pi)}$ values of the set of BMS DAs [6]: green segment.

(ii) $a_2^{(\rho)}$ range from NLC-SR in Ref. [20]: blue segment bounded by blue points in good agreement with the projections of the end points of the green $a_2^{(\pi)}$ segment.

(iii) $a_2^{(\pi)}$ estimates from lattice QCD with next-to-next-to-leading-order (NNLO) and next-to-next-to-next-to-leading-order (N^3LO) matching to the $\overline{MS}$ scheme [3]: red segment and interval between the smaller red end points, respectively.

(iv) $a_2^{(\rho)}$ from the lattice calculation in Ref. [22]: red segment at the upper end of the vertical axis.

(v) NLC-SR platykurtic π and $\rho^{\parallel}$ DAs [17,19]: yellow dots on the horizontal and vertical axes, respectively.

(vi) The black dots within the green $a_2^{(\pi)}$ and blue $a_2^{(\rho)}$ intervals show the locations of the pion [23] and the $\rho^{\parallel}$-meson [24] DAs, respectively, obtained from a Dyson-Schwinger equations (DSEs) based approach—see Refs. [23] (pion) and [24] (ρ-meson). One notices that the $a_2^{(\pi)} \to a_2^{(\rho)}$ projection and the original $a_2^{(\rho)}$ value do not coincide.

A key observation from this figure is the existence of a boundary for the pion coefficient $a_2^{(\pi)} = A_2^{(\pi)}$ below which the corresponding $\rho^{\parallel}$ coefficient $a_2^{(\rho)}$ becomes negative. Using the estimates for the parameters $M_3, c_1^{(21)}$ given above, cf. Eq. (6), we find

$$A_2^{(\pi)} \approx 0.1 \tag{9}$$

in agreement with Eq. (7).

Let us also emphasize the good correspondence in (i) and (ii) between the segments of $a_2^{(\pi)}$ and $a_2^{(\rho)}$ derived from NLC-SR. This circumstance makes it tempting to derive a relation similar to Eq. (3) within the NLC-SR approach for the pion [6,20] and the $\rho^{\parallel}$ meson [19–21]. We start with the generalized sum rules for the π and ρ-meson channels. Taking recourse to the sum rules for the pion in the axial channel and for the ρ-meson in the vector channel [20] [Eqs. (7) and (8) there], we write

$$\varphi_\rho^{\parallel}(x) = \left[\varphi_\pi(x) + \Delta_{A_1\rho'}(x, M^2) - \frac{2}{f_\pi^2}\Phi_S(x, M^2)\right] \times e^{C(M^2)m_\rho^2} \tag{10}$$

with $f_\pi \approx 0.132$ GeV, $f_\rho \approx 0.21$ GeV,

$$C(M^2) = \frac{1}{M^2} + \frac{1}{m_\rho^2}\ln\left(f_\pi^2/f_\rho^2\right). \tag{11}$$

The term $\Delta_{A_1\rho'}$ is determined by the difference of the contributions of the higher resonances in the phenomenological parts of the QCD SR for the axial and vector channels:

$$\Delta_{A_1\rho'}(x, M^2) = \left(\frac{f_{A_1}}{f_\pi}\right)^2 e^{-m_{A_1}^2/M^2}\varphi_{A_1}(x) - \left(\frac{f_{\rho'}}{f_\pi}\right)^2 e^{-m_{\rho'}^2/M^2}\varphi_{\rho'}(x). \tag{12}$$

Here, M^2 is the Borel parameter within a stability window to be determined later in accordance with the standard QCD SR practice [25] in such a way as to best reproduce the DA moments. Strictly speaking, Eq. (10) should be considered *in the weak sense*, i.e., for smooth convolutions on *both* sides within the stability domain of M^2; see, for instance, Refs. [6,20].

The expression for $\Phi_S(x, M^2)$ together with some explanations is given in Appendix A (see also Refs. [6,26]), while the decay constants of the next resonances have the values

$$f_{A_1} \approx 0.21\,\text{GeV}, \quad f_{\rho'} \approx 0.175\,\text{GeV} \tag{13}$$

and have been determined in Refs. [6,20], respectively. The dependence of the scalar NLC $\Phi_S(x, M^2)$ on the Borel scale M^2 and the quark virtuality $\lambda_q^2 = 0.4$ GeV^2 is given graphically in Fig. 2, making use of the simplest Gaussian model for the QCD vacuum from Refs. [8,12].

Let us now consider the origin of the difference between $\varphi_\rho^{\parallel}$ and φ_π ensuing from the particular structure of Eq. (10). The term $\Delta_{A_1\rho'}$ represents a simple phenomenological contribution that takes into account the difference of the higher resonances in the vector and axial channels as expressed by their decay constants; cf. Eq. (12). In contrast, the appearance of the term $\frac{2}{f_\pi^2}\Phi_S(x, M^2)$ represents an evident dynamical manifestation of the distinct character

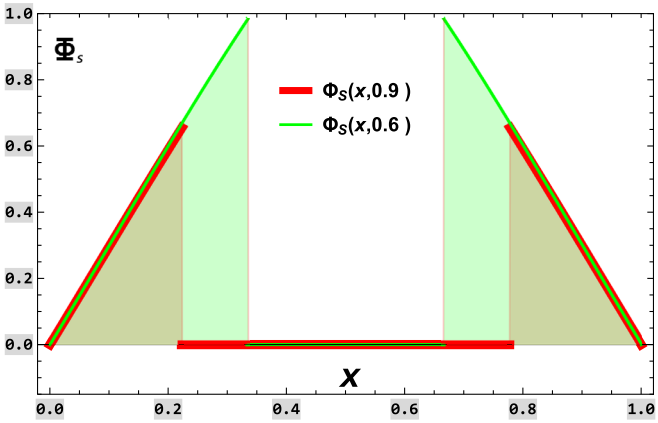

FIG. 2. Scalar condensate $\Phi_S(x, M^2)$ as a function of $x \in [0, 1]$ using the value $\lambda_q^2 = 0.4$ GeV^2; see Ref. [6]. The lighter shaded areas correspond to $M^2 = 0.6$ GeV^2, and the darker shaded areas correspond to $M^2 = 0.9$ GeV^2. An analogous notation is used for the thinner (green) and thicker (red) lines.

of interaction of the scalar vacuum condensate in these two channels. Moreover, it is usually the dominant contribution.

What is the physical reason for the dynamical difference, encoded in $-2\Phi_S$, between $\varphi_\rho^\parallel$ and φ_π in Eq. (10)?

The pion DA φ_π is extracted from the axial-axial correlator because it originates as the pion projection of the *axial* (nonlocal) current, while the $\varphi_\rho^\parallel$ DA is extracted from the vector-vector correlator because it is the ρ-meson projection of the (nonlocal) *vector* current.

The scalar NLC is the only vacuum condensate, among others included in the used approximation, whose contribution is affected by the gamma-matrix structure of the coefficient function. All other condensate contributions to the theoretical part of the QCD SR are the same for both channels, i.e., axial-axial and vector-vector, of these correlators and are accumulated in φ_π. As a result, the repeated commutations of γ_5 with an axial vertex change the sign of the coefficient function of the scalar condensate relative to a chain of commutations with vector vertices. We will discuss the implications of these effects for the ρ and π DAs in Sec. IV.

Mathematically, Eq. (10) generates a linear relation between any (linear) functionals depending on the DAs $\varphi_\rho^\parallel$ and φ_π. This means that if such a relation holds for the ρ-meson DA this functional can be replaced by the rhs of Eq. (10), where the π DA and Φ_S enter.

For our further considerations, it is useful to make use of the convolution

$$\varphi_{\rm M} \otimes f = \int_0^1 \varphi_{\rm M}(x) f(x) dx. \tag{14}$$

Then, we can employ the Gegenbauer expansion of the meson DA $\varphi_{\rm M}$ in Eq. (1) to get expressions in terms of the coefficients a_n of meson M,

$$a_n^{\rm M} = \varphi_{\rm M} \otimes \tilde{\psi}_n = \int_0^1 \varphi_{\rm M}(x) \tilde{\psi}_n(x) dx, \tag{15}$$

where $a_n^{\rm M}$ are the coefficients of the "conformal expansion" over the adjoint harmonics

$$\tilde{\psi}_m(x) = C_m^{3/2}(2x-1)/N_m, \tilde{\psi}_m \otimes \psi_n = \delta_{nm} \tag{16}$$

and $N_m = 3(m+1)(m+2)/2(2m+3)$ are normalization constants.

Convoluting expression (10) with $\tilde{\psi}_m(x)$, we obtain

$$a_n^{(\rho)} \overset{\rm sr}{=} \left[a_n^{(\pi)} + \Delta_{A_1\rho'} \otimes \tilde{\psi}_n - \frac{2}{f_\pi^2}\Phi_S \otimes \tilde{\psi}_n\right] e^{C(M^2)m_\rho^2}, \tag{17}$$

in which the last term in the square brackets dominates over the second one. For example, for $n=2$, the second "resonances" term contributes only a few % compared to the scalar NLC. The notation $\overset{\rm sr}{=}$ means that one should take the average of the rhs over M^2 within the stability window in the Borel parameter, i.e.,

$$0.55\ {\rm GeV}^2 = M_-^2 < M^2 \lesssim M_+^2 = 1.1\ {\rm GeV}^2,$$

in order to obtain a certain numerical value of the lhs.

III. CONNECTION BETWEEN SCALAR NLC AND PION PDF

In this section, we work out relation (17) for the second and fourth meson moments in connection with the NLC-SR and its vacuum parameters. To this end, all scale-dependent quantities are evolved from $\mu^2 = 4\ {\rm GeV}^2$ to the typical scale of QCD SR $\mu_0^2 \simeq 1\ {\rm GeV}^2$ using the NLO evolution procedure described in Ref. [16] (see also Refs. [19,21]).

A. $\rho^\parallel - \pi$ relation for the $a_2^{\rm M}$ moment

For $n=2$, Eq. (17) looks as the analog of Eq. (3) expressed in terms of the Borel-mass dependent NLC-SRs. For this reason, also the elements in the rhs of (17) depend on the parameter M^2. Let us now confront the meaning and estimates of the different elements of this SR with their counterparts in Eq. (3). Evaluating the above expression for $n=0$ and supposing that the normalization conditions $a_0^{(\pi)} = a_0^{(\rho)} = 1$ hold *within a common window of stability* with respect to M^2, we find

$$\left[1 + \Delta_{A_1\rho'} \otimes \tilde{\psi}_0 - \frac{2}{f_\pi^2}\Phi_S \otimes \tilde{\psi}_0\right]^{-1} = e^{C(M^2)m_\rho^2}, \tag{18}$$

where $\tilde{\psi}_0 = 1$. This equation can be used to estimate the "constant" $C(M^2) = C$, which has a physical sense similar to $c_1^{(21)}$ in Eq. (3). However, the sum rule (18) for C is unstable and can only provide the domain of variation of $C \in [0.8 - 0.2]$. Nevertheless, this interval has some overlap with the estimate for the subtraction constant $c_1^{(21)} \in [0.7 - 0.9]$ calculated in Ref. [1].

It is useful to rewrite relation (17) by expressing the factor $e^{C(M^2)m_\rho^2}$ through the lhs of (18) to obtain the more homogenous form

$$a_n^{(\rho,sr)} \overset{\rm sr}{=} \left[a_n^{(\pi)} - \left[\frac{2}{f_\pi^2}\Phi_S - \Delta_{A_1\rho'}\right]_n\right]\mathcal{N}(M^2) \tag{19a}$$

$$\mathcal{N}(M^2) \overset{\rm sr}{=} \left[1 - \left[\frac{2}{f_\pi^2}\Phi_S - \Delta_{A_1\rho'}\right]_0\right]^{-1}, \tag{19b}$$

where $[\Delta_{A_1\rho'}]_n \equiv \Delta_{A_1\rho'} \otimes \tilde{\psi}_n$, $[\Phi_S]_n \equiv \Phi_S \otimes \tilde{\psi}_n$, and $\mathcal{N}(M^2)$ is a normalization factor. It is worth noting that relation (19a) for $n=2$ possesses a sufficient stability with respect to M^2 and finally yields for $a_2^{(\pi)}(\mu_0^2) = 0.187$ [6] (used as input for the evaluation of the rhs) the result $a_2^{(\rho,sr)}(\mu_0^2) = 0.047^{+0.035}_{-0.011}$. This estimate agrees with the

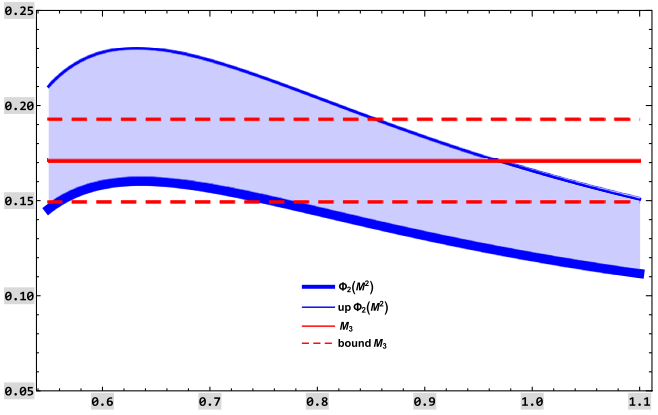

FIG. 3. The central solid (red) line represents the mean value of M_3 (y axis) $\frac{7}{6}M_3 = 0.171(22)$ at μ_0^2 (using the more precise lattice estimate from Ref. [5]), while the dashed (red) lines mark its uncertainties from Ref. [4]. The thick (blue) line depending on M^2 (x axis) is the rhs of Eq. (22) before averaging, i.e., $\Phi_2(M^2)$, whereas the upper thinner (blue) line denotes its upper limit [27] (see Appendix B).

value $a_2^{(\rho)}(\mu_0^2) = 0.047(58)$ obtained from the original NLC-SR in [21] but is more accurate.

We are now in the position to relate the moment expressions, obtained within the two considered nonperturbative approaches to the QCD vacuum, using the scalar condensate. Evaluating Eq. (19) for $n = 2$ and averaging the rhs over M^2, we obtain

$$a_2^{(\rho,sr)} = [a_2^{(\pi)} - \langle\Phi_2\rangle]\langle\mathcal{N}\rangle,$$
$$a_2^{(\rho)} = \left[a_2^{(\pi)} - \frac{7}{6}M_3^{(\pi)}\right] e^{(c_1^{(21)} m_\rho^2)}, \tag{20}$$

where we have shown in the second line Eq. (3) from Ref. [1] for convenience. Here, we employed the notation

$$\Phi_n \equiv \left[\frac{2}{f_\pi^2}\Phi_S - \Delta_{A_1\rho'}\right]_n \frac{\mathcal{N}}{\langle\mathcal{N}\rangle}, \tag{21a}$$

where $\langle f\rangle$ denotes the average over the stability window of M^2:

$$\langle f\mathcal{N}\rangle = \int_{M_-^2}^{M_+^2} f(x)\mathcal{N}(x)dx/(M_+^2 - M_-^2). \tag{21b}$$

To get the same outcome from expressions (20) and (3), we have to conclude that

$$\frac{7}{6}M_3 \approx \langle\Phi_2\rangle. \tag{22}$$

Evolving the estimate in Eq. (6) to the scale μ_0^2, we obtain for the lhs of (22) the value 0.171(22) [5], which is shown as a solid line in Fig. 3 together with its uncertainties denoted by dashed red lines. The quantity $\Phi_2(M^2)$ together with its upper boundary is displayed by means of the shaded (blue) strip that has a strong overlap with the dashed (red) lines. The mean value of $\Phi_2(M^2)$ varies in the range $\langle\Phi_2\rangle = 0.139 \div 0.196$ so that for (22) we have

$$\text{Eq. (22)} \Rightarrow \begin{cases} \text{lhs}: 0.171(22) \\ \text{rhs}: 0.139 \div 0.196 \end{cases} \tag{23a}$$

$$\text{lhs}: 0.171(22) \approx \text{rhs}: 0.167(29), \tag{23b}$$

where in the rhs of (23b) we employed the mean value of the interval in (23a). Note that the uncertainties in the estimate of Φ_2 are entailed by the uncertainties of the value of the quark condensate $\langle\sqrt{\alpha_s}\bar{q}q\rangle^2$ and the use of the single parameter λ_q^2, cf. Eq. (8), to describe correlations in the quark NLC; see Appendix A.

These considerations establish the approximate validity of Eq. (22). This equation represents an intriguing relationship between the measurable quantity M_3 (the third moment of the pion PDF) and the scalar NLC Φ_S which parametrizes the nontrivial vacuum of QCD. Let us recall here that Φ_S significantly dominates in the rhs of (22), while the lhs of this equation was obtained by appealing to the general properties of QFT that gave rise to the nontrivial relation (3) derived in Ref. [1]. It involves no further assumptions or theoretical modeling.

From this perspective, the condition for the sign of $a_2^{(\rho)}$ in Eq. (7) turns out to be directly related to the QCD vacuum characteristics in terms of the mean value of the scalar condensate,

$$\text{If } a_2^{(\pi)}(\mu_0^2) \geq \langle\Phi_2\rangle (= 0.167)$$
$$\text{then } a_2^{(\rho)}(\mu_0^2) \geq 0, \tag{24}$$

and vice versa. The same condition can be obtained directly from Eq. (3) using the replacement $\frac{7}{6}M_3 \to \langle\Phi_2\rangle$, as illustrated in Fig. 1 (at the scale $\mu^2 = 4$ GeV^2).

B. Conformal expansion beyond second order

Let us start with the sum-rule result in Eq. (19a) evaluated for $n = 4$:

$$a_4^{(\rho,sr)}(\mu_0^2) = [a_4^{(\pi)} - \langle\Phi_4\rangle]\langle\mathcal{N}\rangle. \tag{25a}$$

From the above equation, we can extract the value

$$a_4^{(\rho,sr)} = -0.058^{+0.023}_{-0.020},$$

which corresponds to $a_4^{(\pi)} = -0.129$ (25a) [6,21] in the rhs, while the value of $\langle\Phi_4\rangle$ turns out to be also negative. This value of $a_4^{(\rho,sr)}$ agrees well (with an even better accuracy) with

TABLE I. Estimates of (a_2^ρ, a_4^ρ) at $\mu_0^2 \simeq 1$ GeV^2 based on the results for the *mean values* of (a_2^π, a_4^π) within the NLC-SR [21,26] and independently on Eqs. (20) and (25a).

Meson (**M**)	Source	$a_2^{\mathbf{M}}$	$a_4^{\mathbf{M}}$
$\boldsymbol{\rho}_\parallel$	NLC-SR [21]	0.047(58)	−0.057(0.118)
	Here (20), (25)	$0.047^{+0.035}_{-0.011}$	$-0.058^{+0.023}_{-0.020}$
	Here, based on	⊛ $0.019^{+0.025}_{-0.009}$	−0.027
		As input	for $\rho_\parallel$ DA:
$\boldsymbol{\pi}$	NLC-SR [6,21]	0.187	−0.129
	Model ⊛ [26]	0.159	−0.098

$$a_4^{(\rho)} = -0.057(118)$$

obtained in the standard NLC-SR analysis in Ref. [21]. The expressions for the conformal coefficients for any n in both discussed approaches are given in Appendix B.

In Table I, we present pairs (a_2^ρ, a_4^ρ) computed by using as input some favored pion DAs: (i) BMS model [6] and (ii) a new DA determined in Ref. [26] (denoted there by the symbol ▲). This DA belongs to the BMS family and complies with the latest lattice result [3] at N^{3}LO.

The dispersive approach elaborated in Ref. [2] gives a linear relation analogous to (3) also for the higher conformal coefficients. Based on the results obtained in Ref. [2] (see, also, the discussion in Appendix B), one derives the relation

$$a_4^{(\rho)} = \left[a_4^{(\pi)} - \frac{11}{9} M_5^{(\pi)} - B_{43}\right] \exp\left(c_4 m_\rho^2\right), \tag{25b}$$

where the coefficient $B_{43}(0)$ was determined to be $B_{43}(0) \approx -0.12$, while the low-energy subtraction constant c_4 can only be poorly estimated from the instanton model [2] to have the value $c_4 = 1$ GeV^{-2}. Comparing (25b) with (25a), and assuming the approximate equality

$$\exp\left(c_4 m_\rho^2\right) \simeq \langle \mathcal{N} \rangle, \tag{26a}$$

we claim the validity of the relation

$$\frac{11}{9} M_5^{(\pi)} + B_{43}(0) = \langle \Phi_4 \rangle. \tag{26b}$$

The numerical evaluation of the rhs of Eq. (26b) amounts to the mean value of $\langle \Phi_4 \rangle = -0.069(50)$ within the fiducial window in M^2 (at the normalization scale $\mu_0^2 \simeq 1$ GeV^2). In the lhs of this equation, we can use the estimate for $M_5^{(\pi)} \equiv \langle x^4 \rangle = 0.027(2)$ from the Jefferson Lab Angular Momentum (JAM) PDF in Ref. [5] (at $\mu^2 = 4$ GeV^2) and the estimate for $B_{43}(0)$ so that evolving the lhs to μ_0^2 we obtain for Eq. (26b) the approximate numerical equality (within errors)

$$\text{lhs}: 0.049(4) - 0.12 = -0.071(4) \approx \text{rhs}: -0.069(50) \tag{27}$$

to complete the comparison. The reasonable numerical agreement of the estimates in (23) and (27) gives support to the claim that the nonlocal scalar condensate Φ_S and the pion nonsinglet PDF $[q_\pi(x) - \bar{q}_\pi(x)]$ are indeed linearly related to each other. This unexpected result provides the possibility to unravel the basic characteristics of the nonperturbative QCD vacuum using measurements in DIS.

Let us now consider the estimate $c_4 = 1$ GeV^{-2} obtained from the instanton model [2]. For this value, the proposed relation $\exp(c_4 m_\rho^2) \simeq \langle \mathcal{N} \rangle$ in Eq. (26a) cannot be realized. The rhs of Eq. (26b) becomes instead the weighted sum of $\langle \Phi_4 \rangle$ and $a_4^{(\pi)}$ so that

$$\frac{11}{9} M_5^{(\pi)} + B_{43}(0) = \langle \Phi_4 \rangle \frac{\langle \mathcal{N} \rangle}{e^{m_\rho^2 c_4}} + a_4^{(\pi)} \left(1 - \frac{\langle \mathcal{N} \rangle}{e^{m_\rho^2 c_4}}\right). \tag{28}$$

Substituting $a_4^{(\pi)} \approx -0.129$ (see Table I) and $\langle \mathcal{N} \rangle / e^{m_\rho^2 c_4} \approx 0.54$ into the rhs of this equation, we obtain

$$0.049(4) - 0.12 = -0.071(4) \sim \text{rhs}: -0.096(\pm 0.027), \tag{29}$$

where we have neglected the uncertainty of $a_4^{(\pi)}$ and the correlation between the estimates of B_{43} and c_4. From the above considerations, we conclude that Eq. (29) is approximately fulfilled even for this case.

IV. IMPLICATIONS FOR THE $\rho^\parallel$-MESON AND PION DA

Let us now discuss the implications of the cross-link relations derived in the previous sections for the pion and $\rho^\parallel$-meson DAs.

Polyakov and Son claimed in Ref. [1] that the different signs of $a_2^{(\rho)} < 0$ and $a_2^{(\pi)} > 0$ could be regarded as an indication that the corresponding DAs may differ significantly. The origin of this difference could be ascribed to their distinctive response to the nonperturbative structure of the QCD vacuum. To make this difference more explicit, we display below their nonperturbative content in terms of NLCs:

$$\Phi_{\rho(\pi)}(x, M^2) = \mp \Phi_S(x, M^2) + \Phi_{\bar{q}Aq}(x, M^2) + \Phi_V(x, M^2) + \Phi_G(x, M^2). \tag{30}$$

These contributions represent the (i) Φ_S (scalar four-quark condensate), (ii) $\Phi_{\bar{q}Aq}$ (quark-gluon-antiquark condensate), (iii) Φ_V (vector quark condensate), and (iv) Φ_G (gluon condensate), with explicit expressions given in Appendix A of Ref. [28]. One notices that the four-quark condensate enters the expression for the $\rho^\parallel$-meson DA with the opposite sign relative to the π DA. As a consequence, it tends to reduce the relative weight of this condensate with

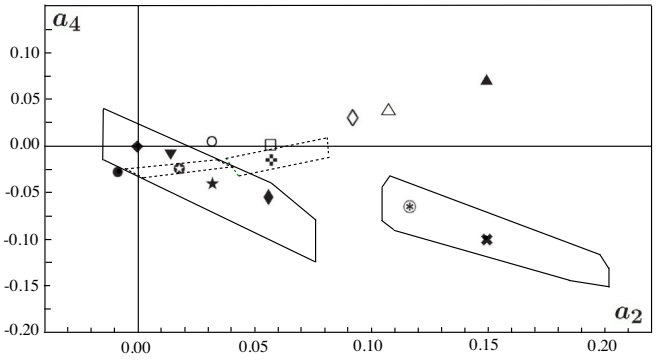

FIG. 4. Snapshot of various π and $\rho^{\parallel}$ DAs from different approaches at the scale $\mu = 4$ GeV^2 in the (a_2, a_4) plane. The large "rectangle" intersecting with the $a_2 = 0$ line denotes the region of $\rho^{\parallel}$ DAs determined with NLC-SR. It encloses the shaded platykurtic regime, where circle white star is the DA determined in Ref. [19]. The symbol filled star refers to the bimodal DAs from NLC-SR in Ref. [21] and filled diamond [20], respectively. The symbol filled black down-pointing triangle represents the $\rho^{\parallel}$ DA from the lightfront model in Ref. [30], and ◆ marks the asymptotic DA. Outside this rectangle, one has the following DAs: Box [31] and diamond [24]. The other large rectangle farther to the right contains the domain of the BMS pion DAs [6] obtained with NLC-SR, with bold times denoting the bimodal BMS pion DA. The pion DA represented by asterisk-circle was determined in Ref. [26] as the crossing point of the long middle line of this rectangle with the lattice result $a_2^{(\pi)} = 0.116^{+19}_{-20}$ at N^{3}LO with three-loop matching to the $\overline{\text{MS}}$ scheme [3]. The dashed rectangle, crossing the $a_4^{(\pi)} = 0$ line, shows the platykurtic range of pion DAs with bold plus marking the DA determined in Ref. [17]. The symbols triangle and filled triangle reproduce, respectively, the DAs obtained within holographic AdS/QCD [32] and a DSE-based approach [23], while ○ shows the pion DA from the instanton model in Ref. [33] after NLO evolution to the scale 4 GeV^2. Similarly, filled circle represents the instanton-based $\rho^{\parallel}$ DA from Ref. [34].

the result that the DA moments (or conformal coefficients) become smaller. This may indeed entail different shapes for these DAs.

For instance, the $\rho^{\parallel}$ DA could have a unimodal shape close to the asymptotic form describing a more or less equal distribution of longitudinal momentum between the two valence quarks, while the nonperturbative effects in the pion could lead to a much broader unimodal or bimodal distribution which favors unequally distributed momentum shares away from $x = 1/2$; see, e.g., Refs. [6,29].

A negative sign prediction for $a_2^{(\rho)}$ is not completely new. In fact, in Ref. [19], it was found that in the case of the two $\rho^{\parallel}$ DAs determined with NLC-SR, notably the platykurtic DA [19] and the DA from Ref. [21], the range of $a_2^{(\rho)}$ *can* indeed be negative; see Fig. 4. However, this possibility was not considered any further. In contrast, the negative sign of $a_2^{(\rho)}$ in Ref. [1] appears as a strict finding of rather general principles of QFT and the instanton model, giving rise to the condition $a_2^{(\pi)}(\mu^2 = 4\ \text{GeV}^2) = 0.078 < 7/6M_3^{(\pi)}$ and, thus, deserves particular attention.

Let us discuss these issues in terms of Fig. 4, which shows the locations of various pion and $\rho^{\parallel}$ DAs in the (a_2, a_4) plane at the scale $\mu^2 = 4$ GeV^2, and apply Eq. (3) in conjunction with Fig. 1. Then, only two classes of $\rho^{\parallel}$ DAs are possible depending on the sign of $a_4^{(\rho)}$. If it is positive, then the corresponding DA will belong to the area above the $a_4^{(\rho)} = 0$ line and will have a profile close to the asymptotic DA. If a_4 is negative, the DA will be located below the $a_4^{(\rho)} = 0$ line and will have an almost asymptotic profile combined with a mild end point suppression. The broadest variant of these $\rho^{\parallel}$ DAs is a platykurtic, i.e., a unimodal distribution with suppressed end points [19], belonging to the embedded dashed rectangle in Fig. 4.

In all considered cases, these DAs will differ substantially from the end-point-suppressed, but bimodal pion DAs within the BMS rectangle [6] shown in this figure in terms of solid lines. The difference between a quasiasymptotic $\rho^{\parallel}$ DA and the end-point-enhanced bimodal Chernyak-Zhitnitsky pion DA [29], obtained with local condensates with $a_2^{\text{CZ}}(2\ \text{GeV}) = 0.42$ [19], is even stronger and is located outside the displayed range of $a_2^{(\pi)}$. Similar considerations as those obtained from the DSE based approach apply also to broad unimodal pion DAs; see Ref. [18] for a recent review. Indeed, from Fig. 4, one sees that the corresponding pion DA, given by ▲, is a broad unimodal distribution differing strongly from the asymptotic one. A similar observation applies also to the pion DA derived in holographic QCD, shown by △. Hence, this scenario supports the assumption that the π and the $\rho^{\parallel}$ interact differently with the nonperturbative QCD vacuum giving rise to very different DAs.

The other possible scenario would allow both meson DAs to have similar shapes. In fact, the $\rho^{\parallel}$-meson DA can be obtained from the pion bilocal correlator by the replacement $\gamma_\mu\gamma_5 \to \gamma_\mu$ [29] so that one may naively think that this does not cause significant changes. The simplest possibility would be that their shapes are both close to φ_π^{asy}; see Fig. 1 in Ref. [19]. But it has been shown by various authors that in this case the pion-photon transition form factor will underestimate the data considerably; see, for instance, Ref. [16] for a recent state-of-the-art analysis based on light-cone sum rules and further references. This implies that the pion DA must be broader than the asymptotic form at experimentally accessible momenta.

The only remaining possibility for these mesons to have similar profiles with $a_2^{(\rho)} < 0$ and $a_2^{(\pi)} > 0$ in combination with pion-photon TFF predictions that agree with most experimental data is that both have $a_4^{(\rho)} < 0$ and $a_4^{(\pi)} < 0$. In this case, their corresponding profiles will have to be platykurtic. As has been shown in Refs. [17,19], and also

more recently in Ref. [26], the platykurtic pion DA reproduces the trend of all data supporting asymptotic scaling at high Q^2 from $Q^2 \geq 1$ GeV^2 up to momenta $\sim$40 GeV^2. The most appropriate numerical values of the conformal coefficients can be extracted by imposing additional constraints from lattice simulations. It is worth noting that the latest lattice calculation of $a_2^{(\rho)}$ in Ref. [22] gives the rather large positive value $0.132(\pm 0.027)$ that is incompatible with the restriction $a_2^{(\rho)} < 0$. On the other hand, employing the most recent lattice constraint on $a_2^{(\pi)}$ with NLO or NNLO accuracy from Ref. [3], one finds from Fig. 1 that $a_2^{(\rho)} \in [-0.01 \div -0.09]$. These lattice constraints can provide in combination with the pion-photon TFF data best-choice parameters $a_2^{(\pi)}$ and $a_4^{(\pi)}$, from their overlapping region as shown in Ref. [16]. However, the new $a_2^{(\pi)} = 0.116^{+0.019}_{-0.020}$ lattice estimate of Ref. [3] at N^{3}LO with three-loop matching to the $\overline{\text{MS}}$ scheme favors a pion DA with a moderate bimodal profile, like ⊛ [26], giving support to the first considered scenario. Further constraints are needed along the upper diagonal in Fig. 4 in order to resolve the fine details of the pion DA more reliably.

V. CONCLUSIONS

In this work, we investigated cross-link relations between the Gegenbauer coefficients of the $\rho^{\parallel}$-meson and pion DAs. We showed that the linear relation between $a_2^{(\rho)}$ and $a_2^{(\pi)}$ obtained recently in Ref. [1] on the basis of rather general assumptions in combination with estimates from the instanton vacuum can also be obtained using QCD sum rules with nonlocal condensates. In fact, we were able to derive an intriguing relation between the third Melin moment of the pion PDF measured in DIS and the scalar condensate [see Eq. (22)]. We also extended this cross-link relation to the next-order Gegenbauer coefficients, establishing further the connection between these two nonperturbative descriptions of the QCD vacuum [see Eq. (26b)]. These findings may contribute to a better understanding of the intrinsic structure of the QCD vacuum by measurements of the pion PDF. The COMPASS++/AMBER experiment at CERN may provide high-precision data for the pion structure function to extract such information.

Adopting a broader perspective, we discussed the general implications for the pion and $\rho^{\parallel}$-meson DAs entailed by the strict application of Eq. (7) by formulating two different generic scenarios. With respect to the space (a_2, a_4), we found that the imposition of $a_2^{(\rho)} < 0$ not only reduces the available range of the $\rho^{\parallel}$-meson coefficients, but it also contributes important constraints for the proper selection of the pion DA. We concluded that either these mesons may have (for whatever reason) very different DAs or, if these are assumed to be similar (for whatever reason), then they can only have a platykurtic, i.e., unimodal profile with suppressed tails [16,17,19,35]. The most recent lattice result from Ref. [3] for $a_2^{(\pi)}$ seems to support at N^{3}LO rather the first scenario, while the analogous estimates at NLO and NNLO conform also with the second option. The possibility that *both* DAs are close to the asymptotic form seems to be excluded because the pion-photon TFF calculated with φ_π^{asy} underestimates the available data considerably demanding a broader distribution for the pion DA.

ACKNOWLEDGMENTS

We would like to thank Maxim Polyakov for inspiring discussions and valuable comments on the manuscript. We have also profited from conversations with Hyeon-Dong Son. S. V. M. acknowledges support from the Heisenberg–Landau Program 2021.

APPENDIX A: NONLOCAL SCALAR CONDENSATE

Application of the factorization ansatz on the four-quark condensate leads to the product of a pair of scalar condensates M_S, where $M_S(z^2) = \int_0^\infty \exp(-z^2/4\alpha) f_S(\alpha) d\alpha$. The correlation functions $f_S(\alpha)$ for each of these scalar condensates determine the distribution in virtuality α of the quarks in the QCD vacuum [12,28]. For example, for $f_S(\alpha;\Lambda,\sigma) \sim \alpha^{n-1} e^{-\Lambda^2/\alpha - \alpha\sigma^2}$, one obtains the expected exponential asymptotic behavior for $M_S(z^2)$ at large z^2: $M_S(z^2) \sim \exp(-\Lambda z)$.

In the NLC approach, the factorization ansatz may lead to an overestimation of the four-quark condensate contribution $\Phi_S(x;M^2)$ because it evidently neglects the correlation between these pairs. The relevant expression within this approximation is given by

$$\Phi_S(x,M^2) = \frac{18 A_S}{M^4} \int\int_{00}^{\infty} d\alpha_1 d\alpha_2 f_S(\alpha_1) f_S(\alpha_2) \times \frac{x\theta(\Delta_1 - \bar{x})}{\Delta_1^2 \Delta_2 \bar{\Delta}_1^2} \left[\bar{x}\Delta_2\bar{\Delta}_1 + \ln\left(\frac{x\Delta_1\bar{\Delta}_2}{x\Delta_1 - (\Delta_1 - \bar{x})\Delta_2}\right) \times \Delta_1(\Delta_1 - \bar{x})\bar{\Delta}_2 \right] + (x \to \bar{x}), \tag{A1}$$

referring for further details to Appendix A in Ref. [28]. The following notations are used: $A_S = (8\pi/81)\langle\sqrt{\alpha_s}\bar{q}(0)q(0)\rangle^2$ and $\langle\sqrt{\alpha_s}\bar{q}q\rangle^2 = (1.84^{+0.84}_{-0.24})\times 10^{-4}$ GeV^6, $\Delta_i \equiv \alpha_i/M^2$, where $\bar{\Delta}_i \equiv 1 - \Delta_i$, and $\bar{x} \equiv 1 - x$. In this work, we used for the NLC estimates the simplest delta-function ansatz $f_S(\alpha) = \delta(\alpha - \lambda_q^2/2)$, proposed in Refs. [8,10,11]; it is sufficient for the accuracy of the moment QCD SRs. This model leads to a Gaussian decay of the scalar quark condensate $M_S(z^2)$ with $\Delta \equiv \lambda_q^2/(2M^2)$:

$$\Phi_S(x;M^2) = \frac{A_S}{M^4}\frac{18}{\bar{\Delta}\Delta^2}\{\theta(\bar{x}>\Delta>x)\bar{x}[x+(\Delta-x)\ln(\bar{x})] + (\bar{x}\to x) + \theta(1>\Delta)\theta(\Delta>x>\bar{\Delta}) \times [\bar{\Delta}+(\Delta-2\bar{x}x)\ln(\Delta)]\}. \quad \text{(A2)}$$

A finite value of Δ, related to the "decay rate" of the correlation length of the NLC [28], shifts the weight of the nonperturbative contributions away from the end points. On the other hand, for $\lambda_q^2 = 0$, all nonperturbative contributions are concentrated just at the end points.

APPENDIX B: RELATIONS BETWEEN THE CONFORMAL COEFFICIENTS $a_n^{(\rho)}$ AND $a_n^{(\pi)}$

We provide here the expressions relating $a_n^{(\rho)}$ to $a_n^{(\pi)}$:

(i) Within the framework of QCD sum rules (label sr) with nonlocal condensates [6,20]:

$$a_n^{(\rho,sr)} = [a_n^{(\pi)} - \langle\Phi_n\rangle]\langle\mathcal{N}\rangle. \quad \text{(B1)}$$

(ii) A similar relation can be obtained within the dispersive approach. Indeed, in Refs. [1,2], the coefficient $a_n^{(\pi)}$ of the conformal expansion was expressed as a sum:

$$a_n^{(\pi)} = \sum_{l=1(\text{odd})}^{n+1} B_{nl}(0). \quad \text{(B2)}$$

Extracting in the sum in the rhs the extreme terms for $l = 1$ and $l = n+1$, notably,

$$B_{n1}(0) = a_n^{(\rho)}\exp(-c_n m_\rho^2), \qquad B_{nn+1}(0) = p(n)M_{n+1}^{(\pi)},$$

one arrives at the expression

$$a_n^{(\rho)} = \left[a_n^{(\pi)} - p(n)M_{n+1}^{(\pi)} - \sum_{l=3}^{n} B_{nl}(0)\right]e^{c_n m_\rho^2},$$
$$p(n) = \frac{3(n+1)}{N_n} = \frac{2(2n+3)}{3(n+2)} \quad \text{(B3)}$$

that can be compared with Eq. (B1).

[1] M. V. Polyakov and H.-D. Son, Phys. Rev. D **102**, 114005 (2020).
[2] M. V. Polyakov, Nucl. Phys. **B555**, 231 (1999).
[3] G. S. Bali, V. M. Braun, S. Bürger, M. Göckeler, M. Gruber, F. Hutzler, P. Korcyl, A. Schäfer, A. Sternbeck, and P. Wein, J. High Energy Phys. 08 (2019) 065; 11 (2020) 037(A).
[4] I. Novikov *et al.*, Phys. Rev. D **102**, 014040 (2020).
[5] C. Alexandrou, S. Bacchio, I. Cloët, M. Constantinou, K. Hadjiyiannakou, G. Koutsou, and C. Lauer, Phys. Rev. D **104**, 054504 (2021).
[6] A. P. Bakulev, S. V. Mikhailov, and N. G. Stefanis, Phys. Lett. B **508**, 279 (2001); **590**, 309(E) (2004).
[7] S. V. Mikhailov and A. V. Radyushkin, Pis'ma Zh. Eksp. Teor. Fiz. **43**, 551 (1986) [JETP Lett. **43**, 712 (1986)].
[8] S. V. Mikhailov and A. V. Radyushkin, Yad. Fiz. **49**, 794 (1988) [Sov. J. Nucl. Phys. **49**, 494 (1989)].
[9] S. V. Mikhailov and A. V. Radyushkin, Yad. Fiz. **52**, 1095 (1990) [Sov. J. Nucl. Phys. **52**, 697 (1990)].
[10] A. P. Bakulev and A. V. Radyushkin, Phys. Lett. B **271**, 223 (1991).
[11] S. V. Mikhailov and A. V. Radyushkin, Phys. Rev. D **45**, 1754 (1992).
[12] A. P. Bakulev and S. V. Mikhailov, Phys. Rev. D **65**, 114511 (2002).
[13] J. Gronberg *et al.* (CLEO Collaboration), Phys. Rev. D **57**, 33 (1998).
[14] S. Uehara *et al.* (Belle Collaboration), Phys. Rev. D **86**, 092007 (2012).
[15] B. Aubert *et al.* (*BABAR* Collaboration), Phys. Rev. D **80**, 052002 (2009).
[16] N. G. Stefanis, Phys. Rev. D **102**, 034022 (2020).
[17] N. G. Stefanis, Phys. Lett. B **738**, 483 (2014).
[18] C. D. Roberts, D. G. Richards, T. Horn, and L. Chang, Prog. Part. Nucl. Phys. **120**, 103883 (2021).
[19] N. G. Stefanis and A. V. Pimikov, Nucl. Phys. **A945**, 248 (2016).
[20] A. P. Bakulev and S. V. Mikhailov, Phys. Lett. B **436**, 351 (1998).
[21] A. V. Pimikov, S. V. Mikhailov, and N. G. Stefanis, Few-Body Syst. **55**, 401 (2014).
[22] V. M. Braun *et al.*, J. High Energy Phys. 04 (2017) 082.
[23] L. Chang, I. C. Cloet, J. J. Cobos-Martinez, C. D. Roberts, S. M. Schmidt, and P. C. Tandy, Phys. Rev. Lett. **110**, 132001 (2013).
[24] F. Gao, L. Chang, Y.-X. Liu, C. D. Roberts, and S. M. Schmidt, Phys. Rev. D **90**, 014011 (2014).
[25] M. A. Shifman, A. I. Vainshtein, and V. I. Zakharov, Nucl. Phys. **B147**, 385 (1979).
[26] S. V. Mikhailov, A. V. Pimikov, and N. G. Stefanis, Phys. Rev. D **103**, 096003 (2021).
[27] S. Cheng, A. Khodjamirian, and A. V. Rusov, Phys. Rev. D **102**, 074022 (2020).
[28] S. V. Mikhailov, A. V. Pimikov, and N. G. Stefanis, Phys. Rev. D **82**, 054020 (2010).
[29] V. L. Chernyak and A. R. Zhitnitsky, Phys. Rep. **112**, 173 (1984).

[30] H.-M. Choi and C.-R. Ji, Phys. Rev. D **75**, 034019 (2007).
[31] M. Ahmady and R. Sandapen, Phys. Rev. D **87**, 054013 (2013).
[32] S. J. Brodsky and G. F. de Téramond, Phys. Rev. D **77**, 056007 (2008).
[33] V. Petrov, M. V. Polyakov, R. Ruskov, C. Weiss, and K. Goeke, Phys. Rev. D **59**, 114018 (1999).
[34] A. E. Dorokhov, Czech. J. Phys. **56**, F169 (2006).
[35] N. G. Stefanis, S. V. Mikhailov, and A. V. Pimikov, Few-Body Syst. **56**, 295 (2015).